Astronomy & Astrophysics manuscript no. paper_NM
July 11, 2025

AT 2023txn (= Gaia23cse): a new and puzzling symbiotic star discovered while outbursting

U. Munari[1], S. Dallaporta[2], P. Valisa[2], N. Masetti[3,4], and A. Maitan[2]

[1] INAF National Institute of Astrophysics, Astronomical Observatory of Padova, 36012 Asiago (VI), Italy
e-mail: ulisse.munari@inaf.it
[2] ANS Collaboration, c/o Astronomical Observatory, 36012 Asiago (VI), Italy
[3] INAF Osservatorio di Astrofisica e Scienza dello Spazio, via Gobetti 93/3, 40129 Bologna, Italy
[4] Departamento de Ciencias Físicas, Universidad Andrés Bello, Fernández Concha 700, Las Condes, Santiago, Chile

Received September 30, 20XX

ABSTRACT

Say something

Key words. binaries: symbiotic – novae, cataclysmic variables – Stars: individual: AT 2023txn – Accretion, accretion disks

1. Introduction

AT 2023txn was first discovered at G=11.83 mag by Gaia on 2023-09-29 as transient Gaia23cse (Hodgkin et al. 2023) at coordinates (J2000) 19:50:33.32 +30:28:22.40. As discussed below in sect. 3.3, the outburst was however already unfurling by at least 19 months when Gaia detected it. A couple of low-resolution optical spectra (range 4000-7500 Ang) were obtained in the immediate aftermath of the Gaia announcement by Fujii et al. (2023), who proposed the object to be a nova. Their spectra show narrow Balmer and FeII emission lines superimposed onto a steeply red continuum.

The transient appears to coincide with source ZTF J195033.33+302822.4, reported by the ZTF catalog of periodic variable stars (Chen et al. 2020) to be a semi-regular variable of 56.18 days period, 0.3mag amplitude, and mean values g=17.136 and r=14.598. The same source is listed also in the second Gaia catalogue of long-period variable candidates (Lebzelter et al. 2023), with no further information. The Gaia DR3 catalog (Gaia Collaboration 2016, 2023) reports for this source B_P=16.20, R_P=11.71, a parallax of 0.1221±0.0397 milliarcsec, and a radial velocity of −62.46±1.61 km s^{-1}, while the values derived from Palomar sky-survey plates and listed in NOMAD (Zacharias et al. 2004) are B=16.76, V=15.28, and R=14.35.

Noting the spatial coincidence with the red giant ZTF J195033.33+302822.4, soon after its announcement we started a monitoring campaign of AT 2023txn, in the prospect it could turn out to be a previously unknown symbiotic star revealed by the current outburst. Symbiotic stars (SySts) are interacting binaries composed by a red giant (RG) and a white dwarf (WD) (see Munari 2019, for a recent review) which are powered by either accretion through a disk and toward the WD (accreting-only SySts) or by nuclear burning on the surface of the latter of the material previously accumulated (burning-type SySts).

We have been following AT 2023txn photometrically (*BVRI* bands) and spectroscopically (low and high resolution), with an X-ray and UV observation with the *Swift* satellite performed on 2024-01-24. In this paper we report about our observational effort and, combined with existing catalog data, our modeling and classification of the object.

2. Observations

2.1. BVRIgri photometry

BVRI photometry of AT 2023txn has been collected from 2023-10-12 to 2025-07-01 with ANS Collaboration telescopes ID 0310 and 2202, and with the Asiago 67/92cm Schmidt camera, while *gri* photometry has been recorded with ANS Collaboration telescope ID 0311. All bands have been observed on each visit to the object. In all we collected 145 *BVRI* sets distributed on 120 individual nights, and 17 *gri* sets over 16 individual nights. All the photometry has been transformed from the local instantaneous photometric system to the Landolt (1992, 2009) standard system via color equations solved for all frames of each night via a *BVRIgri* reference sequence located around AT 2023txn and extracted from APASS DR8 all-sky survey (see Henden & Munari 2014, for details), with color transformations adopted from Munari et al. (2014). The same reference sequence has been used at all telescope on all nights, ensuing a high degree of homogeneity over the entire photometric dataset. The collected photometric data are listed in Table 1 and Table B.1, where the quoted uncertainties are the total error budget (TEB), which quadratically combine the Poisson error and the error associated with the transformation to the standard system via the color equations (usually the dominating term). The resulting *BVRI* light- and color-curves are plotted in Fig. 1.

2.2. Spectroscopy

Low resolution spectroscopy of AT 2023txn was obtained with the Asiago 1.22m + B&C telescope (range 3200-8000 Å, dispersion 2.31 Å/pix). The detector has been an Andor iDus DU440 CCD camera (2048×512 pixels, 13.5×13.5 μm each), which is characterized by a high near-UV sensitivity. The slit was set to a

Table 1: Our *BVRI* photometry of AT 2023txn. The second columns provides the HJD−2460000. The full table is available only electronically via CDS, a small portion is shown here for guidance on its form and content.

Date	HJD	*B*	*V*	*R*	*I*	ID
2023-10-12.790	230.290	14.415 ±0.010	12.884 ±0.013	11.852 ±0.011	10.721 ±0.016	2202
2023-10-16.748	234.248	14.296 ±0.008	12.744 ±0.005	11.716 ±0.006	10.587 ±0.008	0310
2023-10-17.772	235.272	14.321 ±0.009	12.755 ±0.006	11.720 ±0.005	10.597 ±0.010	0310
2023-10-27.918	245.418	14.488 ±0.013	12.904 ±0.007	11.817 ±0.008	10.668 ±0.010	0310

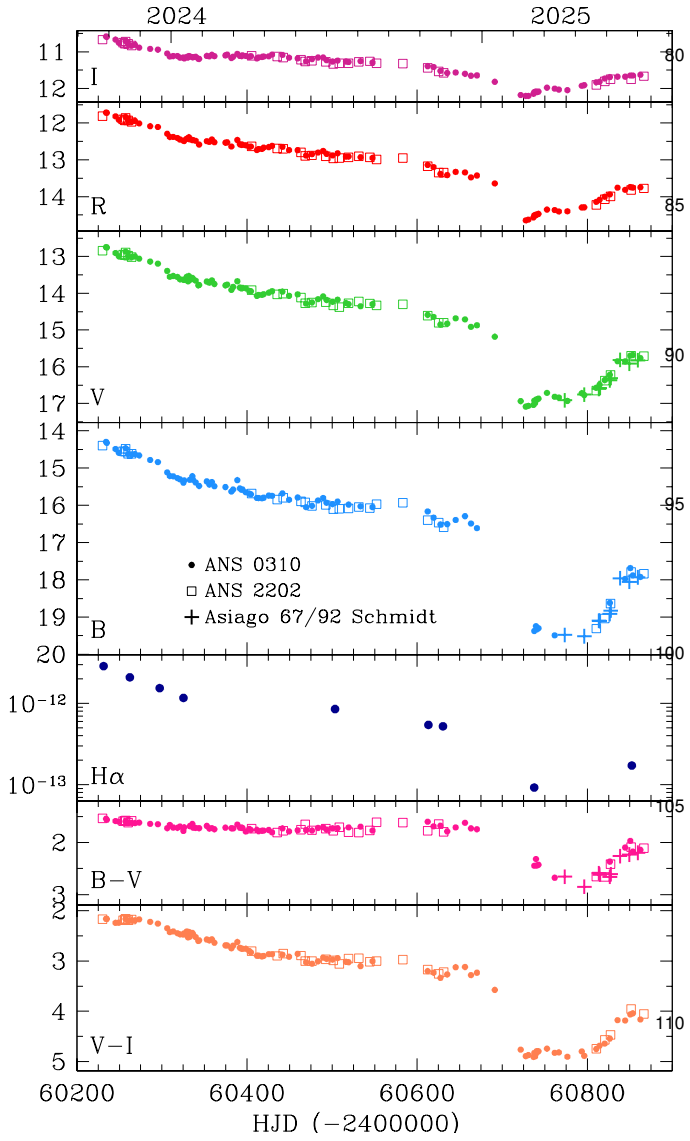

Fig. 1: ANS Collaboration *BVRI* photometry of AT 2023txn over 2023-2025. The Hα panel shows the integrated flux of the Hα emission line measured on the eight Asiago 1.22m + B&C spectra presented in Fig. 2 and on a more recent spectrum obtained on 2025-06-25 with the Varese 0.84m telescope.

width of 2 arcsec and has always been rotated to the parallactic angle for optimal flux calibration against the spectrophotometric standards observed on each night. The slit height of ~8 arcmin allows a careful sampling and subtraction of the sky background. We observed AT 2023txn at eight distinct epochs distributed in time to cover from the maximum brightness during outburst down to the faintest state at the center of the primary eclipse. The absolutely fluxed spectra are presented in Fig 2.

High resolution spectra of AT 2023txn were recorded with the Asiago 1.82m telescope + REOSC Echelle spectrograph. The 3550-7100 Å interval is covered in 32 orders without inter-order gaps by an Andor DW436-BV camera (housing an E2V CCD42-40 AIMO CCD, with 2048x2048 array, and 13.5 μm pixel size). The resolving power is 22,000 for a 1.8-arcsec slit-width. The slit height of 22 arcsec allows recording free 8 arcsec on both sides of the stellar spectrum for a careful definition of the sky background to subtract. Fig. 3 presents the Hα and NaI profiles extracted from these spectra.

Echelle spectra of AT 2023txn were also obtained with the Varese 0.84m telescope, equipped with a long-slit mark.III Multi-Mode Spectrograph from Astrolight Instr. The camera is a SBIG ST10XME CCD and the 4250–8850 Å range is covered in 32 orders without inter-order gaps. A 1×1 binning and 2.0-arcsec slit-width provide a resolving power ~17,000. A final spectrum was obtained at 2×2 binning on 2025-06-27 (resolving power 9,000) when the brightness of the object had much declined compared to outburst maximum. The evolution of the Hα profile as recorded with the Varese 0.84m + Echelle telescope is presented in Fig. 3. With the same telescope and multi-mode spectrograph configured for low-res spectroscopy, a 4300-8600 Å spectrum of AT 2023txn has been recorded at 2.35 Å/pix on 2025-06-25.

Table C.1 provides a comprehensive log book of the spectroscopic observations we collected of AT 2023txn. All spectra acquired with the Asiago and Varese telescopes have been similarly reduced in IRAF, with all standard steps involving correction for bias, dark and flat frames, sky subtraction, wavelength and flux calibration.

2.3. Swift observations

A target-of-opportunity observation of AT 2023txn was performed with the *Swift* satellite (Gehrels et al. 2004) starting at 04:48 UT of January 24, 2024. Data were acquired with the X-Ray Telescope (XRT; Burrows et al. 2005) and the UltraViolet Optical Telescope (UVOT; Roming et al. 2005). The XRT covers the 0.3–10 keV X-ray band, whereas UVOT used the *UVM2* ultraviolet filter, with reference wavelength 2246 Å, (see Poole et al. 2008; Breeveld et al. 2011, for details). The two instruments observed AT 2023txn simultaneously; the XRT pointing lasted 3285 s whereas the UVOT one was 1595 s long. All data were reduced within the FTOOLS environment (Blackburn 1995).

The *UVM2* magnitude of AT 2023txn was measured through aperture photometry within a 10″ radius centered on the source position, whereas the corresponding background was evaluated using a combination of several circular regions in source-free nearby areas on the UVOT image. The choice of an aperture photometry radius larger than usual (5″) was made to address the excess broadening of the UVOT images point spread function produced by issues in the spacecraft attitude control (Cenko 2023, GCN #34633; see also Hussenot-Desenonges et al. 2024, MN-

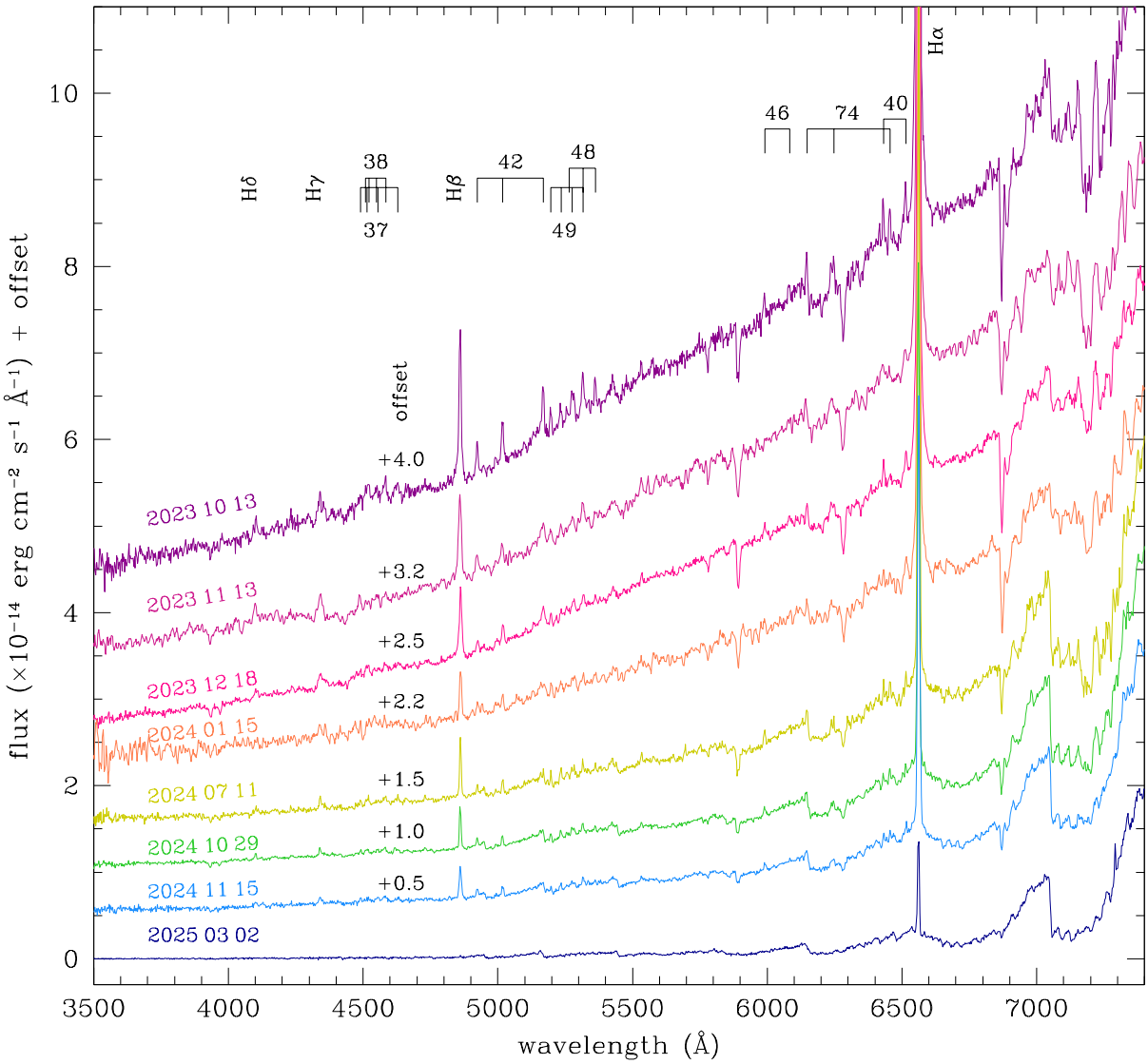

Fig. 2: Spectroscopic evolution of AT 2023txn as tracked with the Asiago 1.22m + B&C telescope, from maximum brightness in October 2023 down to the center of eclipse in March 2025. The strongest emission lines pertain to the hydrogen Balmer series and to FeII multiplets (identified by comb-like markings).

RAS, 530, 1, and Srinivasaragavan et al., 2024, ApJ, 960, L18 about this). The data were then calibrated using the UVOT photometric system described by Poole et al. (2008); the most recent fixings (2020 November) recommended by the UVOT team were taken into account and a check to reject small scale sensitivities[1] was also performed.

AT 2023txn is barely detected in the UVOT image: its $UVM2$ magnitude, determined with the UVOTSOURCE task, is 19.7±0.3. This, assuming a color excess towards the source $E(B-V) = 1.0$ (see Sect. 4) and following the prescription of Kataoka et al.(2008; ApJ, 672, 787; their Table 5) implies a dereddened magnitude $UVM2_0 = 12.5\pm0.3$. These correspond to flux densities of $(6.2\pm1.7)\times10^{-17}$ and $(4.8\pm0.6)\times10^{-14}$ erg cm^{-2} s^{-1} Å^{-1}, respectively.

The XRT data analysis was performed using the XRTDAS standard pipeline package (XRTPIPELINE v. 0.13.4). All X-ray data were acquired in photon counting mode (Hill et al. 2004). Scientific data for AT 2023txn were extracted using a radius of 47″ (20 pixels) centered at the optical coordinates of the source, while the corresponding background was evaluated in a source-free region of radius 94″ (40 pixels). No emission was detected in the 0.3–10 keV range using the XSPEC package down to a 3σ limit count rate of 2×10^{-3} counts s^{-1}, determined using the procedure of Gehrels (1986; ApJ, 303, 336).

We then evaluated the corresponding X-ray flux using the WEBPIMMS online tool[2] by assuming a thermal bremsstrahlung emission with temperature $kT = 2$ keV (see e.g. Luna et al. 2013, A&A, 559, A6) plus an intervening hydrogen column density absorption $N_{\rm H} = 5.5\times10^{21}$ cm^{-2} (obtained adopting again an interstellar reddening $E_{B-V} = 1.0$ along the source line of sight combined with the empirical formula of Predehl & Schmitt (1995). This implies a count rate-to-flux conversion factor of 3.4×10^{-11} erg cm^{-2} s^{-1} counts^{-1} which corresponds to absorbed and unab-

[1] https://swift.gsfc.nasa.gov/analysis/uvot_digest/sss_check.html

[2] https://heasarc.gsfc.nasa.gov/cgi-bin/Tools/w3pimms/w3pimms.pl

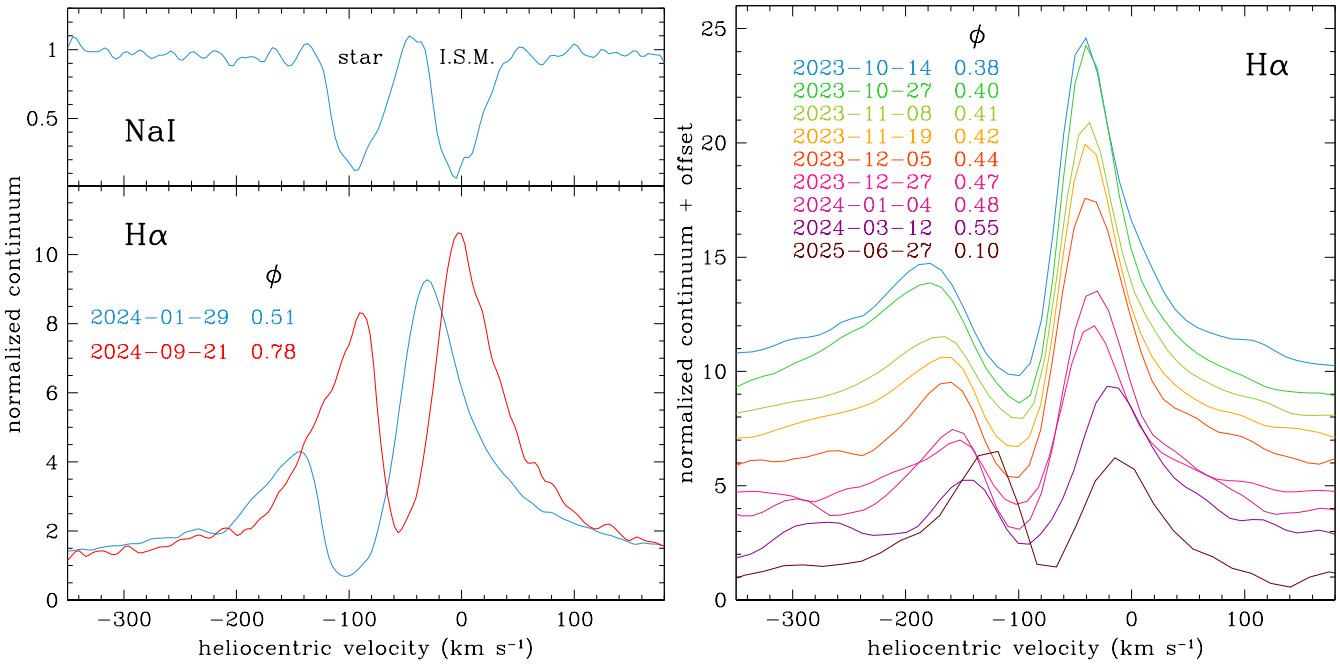

Fig. 3: *Top-left panel*: fully split stellar and interstellar absorption components to NaI 5890 from the Asiago 1.82m + Echelle high-resolution spectrum of AT 2023txn for 2024-01-29. *Bottom-left panel*: Hα profiles of AT 2023txn from the Asiago 1.82m + Echelle high-resolution spectra of 2024-01-29 and 2024-09-21. *Right panel*: evolution of the Hα profile on the Varese 0.84m + Echelle high resolution spectra. All phases ϕ are computed according to Eq. 1.

sorbed flux limits of $<6.7\times10^{-14}$ erg cm^{-2} s^{-1} and $<1.2\times10^{-13}$ erg cm^{-2} s^{-1}, respectively.

3. Long term evolution

3.1. Bulding the sample

AT 2023txn is too faint in quiescence to show up in the Harvard historical photographic plates digitized as part of the DASCH program (Grindlay et al. 2012). The few logged detections (on 13 of the 2017 scanned plates imaging the field containing AT 2023txn) are discussed in Appendix A, and at least several of them appear of dubious nature. Overall, the most convincing detection on historical Harvard plates seems that of 1952, with AT 2023txn being imaged on three distinct plates spanning from August to October, at a mean $<B>$=14.55 brightness in line with the peak value B ~14.3 of the recent outburst.

Combining Gaia, ZTF, our observations, and NeoWISE data it is however possible to reconstruct the photometric evolution of AT 2023txn in the optical and infrared from 2014 to present, and the resulting lightcurves are shown in Fig. 4.

At optical wavelengths, the largest body of data is provided by 2018-2024 g,r patrol photometry from the Zwicky Transient Facility (ZTF; Masci et al. 2019). To extend the time coverage in Fig. 4, we make use of the 2014-2017 B_P,R_P Gaia DR3 photometry and the 2023-2025 B,g,r ANS Collaboration photometry from Table 1 and Table B.1. The photometric evolution of AT 2023txn at infrared wavelengths from 2014 to present is traced in Fig. 4 by W1 and W2 band data (centered respectively at 3.4 μm and 4.6 μm) collected at 6-months interval by the NeoWISE mission (Mainzer et al. 2011, 2014). NeoWISE refers to the data the Wide-field Infrared Survey Explorer (WISE) satellite is collecting since it has been brought out of hibernation and resumed all-sky scanning observation in 2014.

3.2. Quiescence

The 2014-2025 photometric evolution of AT 2023txn presented in Fig. 4 starts with the object being in quiescence up to 2021, showing only a minimal variability in the blue (g) and being rather constant in the red (r) and in the infrared (W1 and W2), which would scarcely qualify the object as the semi-regular variable of 56.18 days period and 0.3mag amplitude logged by Chen et al. (2020), and even less as the Mira variable quoted by Fujii et al. (2023). The mean values in quiescence are $<g>$=17.13, $<r>$=14.61, $<B_P>$=16.20, $<R_P>$=11.71, <W1>=6.89, and <W2>=7.07.

The great photometric stability of AT 2023txn in quiescence - expecially in the infrared where the role of the accretion disk is greatly dimished - argues against the RG filling its Roche lobe, unless we orbital aspect is close to face-on conditions: for mid- to high-inclinations, a Roche-lobe filling RG should display a fairly large ellipsoidal variability, up to ~0.5 mag in amplitude for i~90°, with two maxima and two minima per orbital cycle. The fact that such a modulation is not visible in Fig. 4 ($\Delta W2\leq0.05$ mag) suggests that the RG under-fills its Roche-lobe, impling a wide orbital separation and a mass accretion toward the WD companion occurring via wind-intercept rather than Roche-lobe overflow. It is worth noticing that the Hα profiles in Fig. 3 show a large excursion in radial velocity of both the absorption and the emission components, suggestive of a large-amplitude orbital motion, and therefore a significant orbital inclination well away from face-on conditions.

3.3. Outburst

After the Solar conjunction during December 2021/February 2022, ZTF resumed the observations of AT 2023txn on 2022-03-02 recording the object as much brighter than in precedence and therefore clearly in outburst, but the fact passed unnoticed

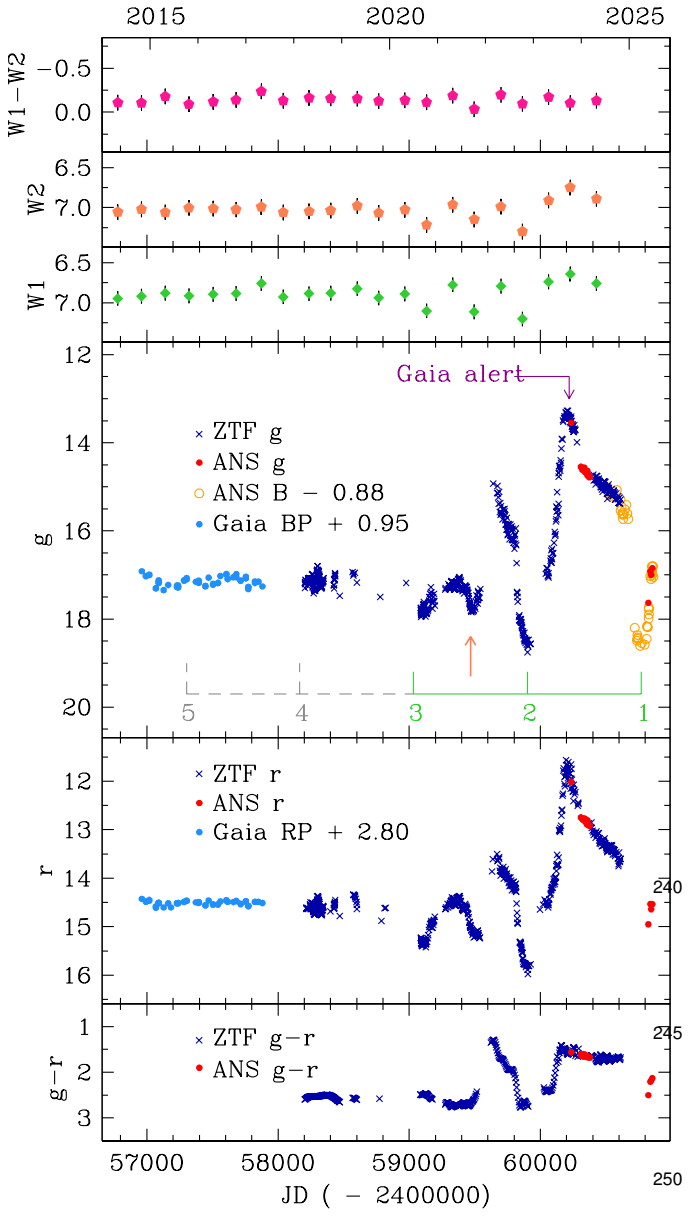

Fig. 4: Long-term photometric evolution of AT 2023txn reconstructed by combining ZTF *gr*, ANS *grB* and Gaia BP,RP photometry. The upper two panels plot the IR photometry collected at 6-months cadence by the NeoWISE satellite in W1 (3.4 μm) and W2 (4.6 μm) bands. The epochs of the eclipses follow Eq. 1.

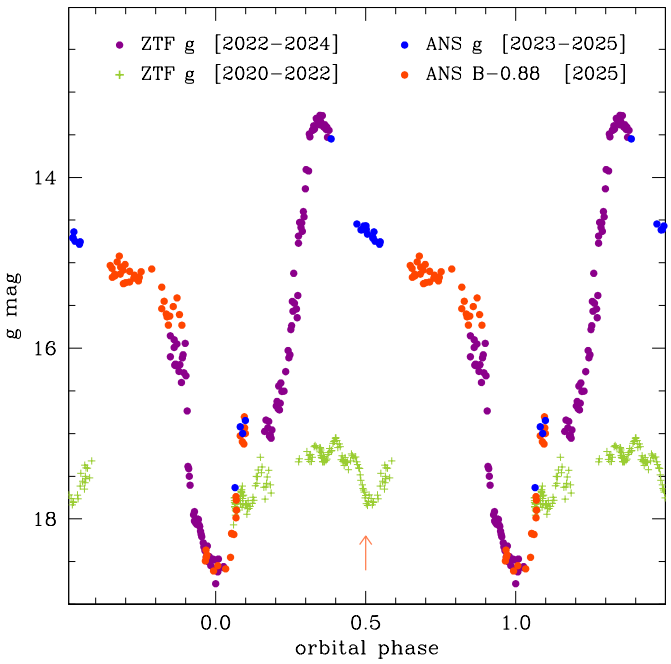

Fig. 5: Phase-reckoned photometry of AT 2023txn to highlight the modulation and eclipses following the orbital period of P=866 days.

and no alert was issued. The protracted outburst of AT 2023txn eventually attracted attention only 19 months later when Gaia detected the object on 2023-09-29, while it was passing at a second and brighter maximum, this time issuing an alert and naming the transient Gaia23cse, which was then logged as AT 2023txn by the TNS[3] server. Even if finally announced, the outburst of AT 2023txn did not rise much attention other than the acquisition of two low-resolution spectra obtained soon after the announcement and uploaded to the TNS server by Fujii et al. (2023), and a single-night *B*,*V* photometry collected by an AAVSO observer (on 2023-11-14, reporting V=13.01, B=14.62).

The lightcurve in Fig. 4 shows that the on-going outburst affecting AT 2023txn has been so far characterized by two maxima, separated by ~565 days, of unequal brightness, preceded by a fast rise, and followed by an initially rapid decline that later progresses at a more sedate rate before plunging into pronounced drops bringing the system brightness below the level in quiescence. The first maximum was reached on 2022-03-02, when ZTF recorded AT 2023txn at g=14.93, r=13.50, with amplitudes with respect to quiescence of Δg=2.20 and Δr=1.11. AT 2023txn passaged at a second and brighter maximum on 2023-09-18 peaking at g=13.27, r=11.60, corresponding to Δg=3.86 and Δr=3.01 compared to quiescence. The decline from second maximum as depicted in Fig. 1 has been particularly smooth in all photometric bands, with mean rates ΔB=0.0071, ΔV=0.0063, ΔR=0.0041, and ΔI=0.0019 mag day^{-1}; while the $V-I$ color reddened at a mean rate +0.0044 mag day^{-1}, the $B-V$ varied much more slowly at just +0.0012 mag day^{-1}.

The spectral evolution of AT 2023txn along the decline from second maximum, which is presented in Fig. 2, has been similarly smooth and gradual as the photometry. The spectrum for 2023-10-13, obtained close to maximum brightness, is dominated by a featureless continuum steeply rising toward the red, and by sharp and low-ionization emission lines from the hydrogen Balmer series and various FeII multiplets (primarily 37, 38, 40, 42, 46, 48, 49, and 74). Hints of the TiO molecular absorption bands from the red giant are discernible only longword of 6900 Å, while the absorption features at bluer wavelengths all originate from the interstellar medium, like the CaII K and NaI atomic lines and the rich ensemble of diffuse interstellar bands (DIBs), in particular those at 4066, 4429, 4970, 5780, 6177, 6281, and 6359 Å, which combined with the steep red color of the continuum suggest high reddening conditions (see sect. 4 below).

The spectroscopic evolution along the decline from maximum can be fairly well described as (*i*) a diminution in the veiling of the RG spectrum by a hotter continuum, and (*ii*) a simple and progressive reduction in the flux radiated by the emis-

[3] https://www.wis-tns.org/

sion lines, without appreciable changes in the ionization degree: they remained sharp, characterized by low ionization conditions, and dominated by FeII and the Balmer series. The evolution of the integrated flux of Hα presented in Fig. 1 is representative of the rest of the emission lines, with a mean decline of 0.004 mag day^{-1} which is comparable to the mean decline in the *BVRI* photometric bands.

Also the profiles of the emission lines remained self-similar during the decline from maximum, as well illustrated by the Hα profiles in Fig. 3 which display an emission with superimposed a blue-shifted absorption component, as typical of symbiotic stars (see eg. Van Winckel et al. 1993, for an atlas of high-resolution profiles of emission line in SySts). The absorption component usually originates in the outflowing wind of the RG that encompasses the central binary, sharing the same orbital motion of the RG and being normally blue shifted from it by the amount of wind terminal velocity (Munari 1993), with the profile for 2024-09-21 in Fig. 3 conforming to such arragment. Any wind blowing off the WD and/or the accretion disk, a condition easier to encounter during bright phases, would add its own absorption signature leading to a broader and structured absorption component, as it is the case for the 2024-01-09 profile in Fig. 3.

3.4. Deep minima

A striking feature of the 2014-2025 lightcurve in Fig. 4 are the deep minima centered on JD 2460768, 2459902, and 2459036 (numbered N.1, N.2, and N.3 in the figure), during which AT 2023txn went well below the brightness in quiescence. Such minima, absent prior to 2021, started showing up at the same time the object entered the outburst season. The minima appear regularly spaced following the ephemeris:

$$\mathrm{Min}(g, B) = 2459902 + 866 \times E \quad (1)$$

which would predic a new event for August 2027. The minima are phase-plotted in Fig. 5, showing a high degree of coherence, as one would expect in case of eclipses of the hot component by the red giant. An eclipse scenario would also nicely agree with the shape of the last minimum, densely convered by the *BVRI* photometry of Fig. 1, and would also naturally account for the pure red giant spectrum that AT 2023txn has displayed during the last minimum (see Fig. 2, Fig. 6, and sect. 5 below).

The interpretation in terms of eclipses faces however with strong difficulties in relation to the absence of minima at earlier epochs, those marked N.4 and N.5 in Fig. 4. Given the Δg=1.5 mag amplitude of the deep minima, the hot component (WD + accretion disk) must contributes about 75% of the total system brightness in quiescence at blue wavelengths, and there is no easy way to justify for the missing minima.

An explanation alternative to that of the hot component being eclipsed by the red giant appears as a necessity, and focusing on the temporal simultaneity between the appearance of minima and of the outburst could pave the way to a solution. We will return to that later, in sect. 8.

4. Reddening

The very red colors for AT 2023txn and the low galactic latitude suggest a large interstellar reddening affecting the object.

Several diffuse interstellar bands are prominent in the Echelle spectra recorded with the Asiago 1.82m telescope. The equivalent width of DIB 5780 is 0.51 Å, and the corresponding reddening is E_{B-V}=1.00 following the calibration by Kos & Zwitter (2013). That of DIB 6614 is 0.24 Å, which leads to E_{B-V}=1.05 according to the relation by Munari (2014). The interstellar NaI line is clearly saturated in the profile presented in the top panel of Fig. 3 and cannot be used, while the equivalent width of interstellar KI 7699 Å measured on the Echelle spectra recorded with the Varese 0.84m telescope is 0.246 Å which corresponds to E_{B-V}=0.98 following Munari & Zwitter (1997). The averaged value E_{B-V}=1.0±0.05 will be adopted in this paper. Such value compares well with the 3D Galactic extinction maps of Sale et al. (2014) and Green et al. (2019), both suggesting $E_{B-V}\geq$0.9 at 7.5 kpc distance along the line-of-sight to AT 2023txn.

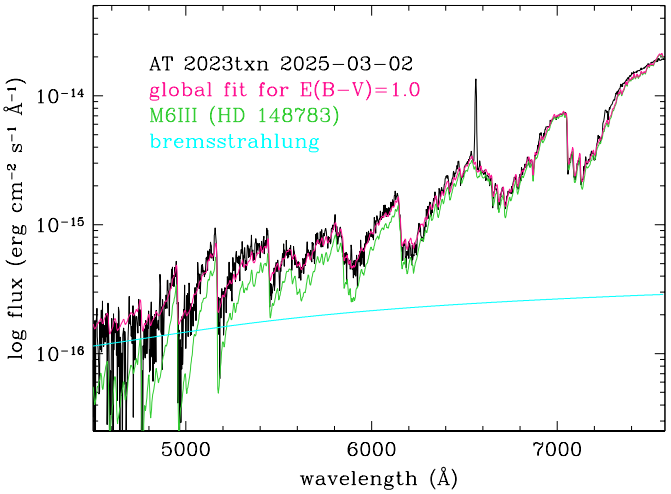

Fig. 6: Fit to the Asiago 1.22m + B&C spectrum for 2025-03-02 obtained right at the center of the eclipse. The spectrum for the scaled M6III template has been obtained with the same telescope, while the bremsstrahlung radiation is computed for an electronic temperature of 10^4 K, and the applied reddening law is that of Fitzpatrick (1999).

5. Spectral type of the red giant

The 2025-03-02 spectrum of AT 2023txn in Fig. 2, which has been obtained right at the center of the deep minimum N.1, is dominated by the emission of the RG, and it is therefore well suited to derived its spectral classification. This spectrum is replotted on an expanded and logarithmic scale in Fig. 6. The S/N at the bluest wavelengths is poor as it may be expected given the faintness of the system shining at B=19.5 mag while transiting at N.1 minimum, requiring a telescope much larger than the Asiago 1.22m telescope we had available for that observation. Nonetheless, the molecular bands longword of 5000 Å are well defined and allow a robust determination of the spectral type and a simultaneous check on the interstellar reddening by fitting with MKK primary spectral standards (selected from Morgan et al. 1943; Morgan & Keenan 1973; Yamashita & Nariai 1977), that we observed with the same equipment used for AT 2023txn. All such standard stars are close to the Sun and suffer from a small or negligible reddening; whatever small, prior to the comparison with AT 2023txn, their spectra were reddening corrected by adopting the R_V=3 reddening law of Fitzpatrick (1999) and the individual E_{B-V} from Hoffleit (1991).

The best fitting to the 2025-03-02 spectrum of AT 2023txn in Fig.6 is provided by an M6III standard (HD 148783), reddened by E_{B-V}=1.0, with a small contribution by a hot continuum (rep-

resented in the figure by the T_e=1×10^4 K bremsstrahlung distribution) which is appreciable at the shortest wavelengths. The requirement about a faint hot continuum is in agreement with the fact that a weak emission in Hα remains visible even at the core of the deep minima, indicating that some fraction of the ionized material remains visible during eclipse. The E_{B-V}=1.0 required by the fit in Fig.6 is in excellent agreement with the reddening determined in sect. 4 from entirely independent methods, which reinforce confidence on both the E_{B-V} and the spectral classification derived by the fitting in Fig. 6.

6. Distance

The small parallax (0.1221±0.0397 mas) listed in Gaia DR3 indicates a large distance to AT 2023txn (at least several kpc). The associated error (33%) is however too large for an entirely safe inversion of the parallax to derive an accurate value for the distance; to achieve that Bailer-Jones (2015) and Luri et al. (2018) recommend an error on the parallax not exceeding 20%.

To estimate the distance to AT 2023txn we may compare it with SU Lyn, a prototype for accreting-only symbiotic stars, that harbors a similar M6III red giant and which suffers from a low E_{B-V}=0.05±0.02 (Mukai et al. 2016). SU Lyn is nearby and therefore its Gaia DR3 parallax is highly accurate at 1.373±0.063 mas (4% error), which fixes the absolute 2MASS K_S magnitude of SU Lyn to M(K_S)=−7.72±0.11, where the error propagates the uncertainties on K_S, the parallax and the reddening. Assuming that the M6III giant in AT 2023txn is characterized by the same M(K_S) of the M6III giant in SU Lyn, the distance to AT 2023txn turns out to be 7.5±0.3 kpc, a value that we will adopt in the rest of this paper (and which is not too far from the 8.2 kpc coming from the straight inversion of the Gaia DR3 parallax). At a Galactic latitude of $|l|$=2°.038, the corresponding height above the galactic plane is 265 pc, while the Gaia DR3 tangential motion of 1.62 mas yr^{-1} translates to a tangential velocity of 57 km s^{-1}, while the system radial velocity reported in Gaia DR3 is −62.1 km s^{-1}.

7. Spectral energy distribution and outburst luminosity

The spectral energy distributions (SEDs) of AT 2023txn around outburst maximum and in eclipse are compared in Fig. 7 to that of an M6III template. A distance of 7.5 kpc and a reddening E_{B-V}=1.0 are adopted from the previous sections. The SED of the reference M6III is built from the intrinsic colors listed by Bessell (1990), Koornneef (1983), Lee (1970), and Wu et al. (1982), scaled to the de-reddened 2MASS K_s magnitude of AT 2023txn.

To derive the energy distribution around maximum we use the *Swift* UVOT-M2 observations of 2024-01-24 and combine it with our *BVRIgri* data obtained within days of the *Swift* visit on AT 2023txn. By integrating the difference in Fig. 7 between the SED of AT 2023txn for 2024-01-24 and the SED of the reference M6III standard, we obtain as the luminosity radiated between 2000 and 9000 Å at the peak of the outburst

$$L^{2000-9000\ \text{Å}}_{\text{outburst peak}} = 5.9 \times 10^{36}\ \text{erg s}^{-1} = 1500\ \text{L}_\odot \quad (2)$$

Given the fact that we did not explore shortward of the UVOT-M2 filter, this is to be considered as a lower limit to $L_{\rm bol}$. Considering that the ionization degree of the emission line spectrum is rather low (just Balmer and FeII are visible) and the <1 L$_\odot$ upper limit to extinction-corrected X-ray emission derived in sect. 2.3, the true value for $L_{\rm bol}$ should not be much larger than given in Eq. 2.

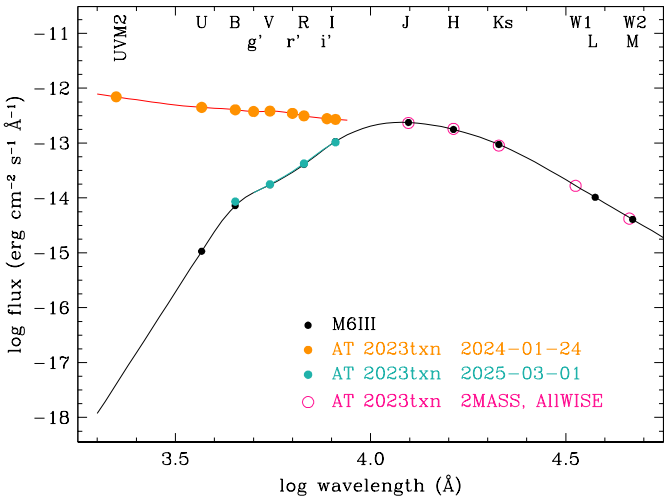

Fig. 7: Spectral energy distribution (SED) of AT 2023txn at the epoch of the *Swift* UVM2 observation (2024-01-24, close maximum brightness) and at the center of the eclipse (2025-03-01). The 2MASS *JHK* and AllWISE W3,W4 data are not simultaneous with the rest. The SED at the center of eclipse is identical to that of the template M6III, except for a minimal excess visible in *B* band and in agreement with the amount of bremsstrahlung radiation required by the fit in Fig. 6.

We have no UVOT observation of AT 2023txn collected around the minimum brightness reached around March 1, 2025 (it would have been anyway too faint for detection by *Swift*, with an estimated UVOT-M2∼26.5 mag), only our *BVRI* observations are available to constrain the SED during eclipse. Plotted in Fig. 7, they confirm that during the deep minima the SED of AT 2023txn is completely dominated by the M6III alone, with the small contribution from the bremsstrahlung emission in Fig. 6 appearing a the small excess at *B* band in Fig. 7.

8. The nature of the outburst and of the eclipses

There are no spectra available for AT 2023txn during quiescence from which to infer the status of the WD and the accretion disk. They must have been however relatively cold, displaying no significant emission in Hα, considering that the IPHAS survey (Barentsen et al. 2014) measured AT 2023txn in June 2004 at Hα=13.89, r=14.90, i=12.26 (compared with Fig. 4, such a value for r means that AT 2023txn was at the time in quiescence). Comparing with the distribution of known symbiotic stars on the IPHAS [r−Hα]/[r−i] plane (Drew et al. 2005; Corradi et al. 2008, 2010; Rodríguez-Flores et al. 2014) the reddening-corrected position of AT 2023txn lies much closer to that of bare M giants than to classical symbiotic stars.

Overall, the situation of AT 2023txn in quiescence seems similar to that of T CrB during the protracted quiescence following the eruption of 1946 as investigated by Munari et al. (2025, A&A submitted): a massive and cold accretion disk, brighter that the RG by ∼1 mag in B band and unable to power emission lines other than a weak Hα, quietly grew in mass for ∼70 yrs without transferring much of that to the WD. The majority of the accumulated mass was finally transferred to the WD in a ∼8 yrs period when the disk, grown beyond stable conditions, flushed

toward the WD most of its content during the so called super-active accretion phase (SAP), giving rise to a surge in system's brightness and in the intensity of emission lines.

Explanations for the outburst of AT 2023txn other than an instability in the accretion disk are improbable:

- the rise-time to maximum, the low ionization conditions, the limited amplitude, the narrow emission lines, and the presence of multiple-maxima exclude an interpretation of the outburst of AT 2023txn in terms of nuclear burning in degenerate conditions, i.e. a nova eruption (see Munari 2025, for a review of the eruption of novae in symbiotic binaries).
- also a nuclear burning igniting is non degenerate conditions, i.e. developing in thermal equilibrium, is similarly contradicted by the observations. Such an event normally takes years to reach maximum power and lasts for decades to centuries, as long as enough hydrogen fuel is present in the shell accreted by the WD (Iben 1982; Fujimoto 1982b,a; Kenyon & Truran 1983).
- the 'Z-And' type of outbursts are observed in SySts undergoing stable H-burning on their WD, and are probably triggered by localized mass-transfer from the disk or the red giant to the burning shell that reacts by expanding in radius and shifting from ultraviolet to optical range the peak of its emissivity. The 3-mag amplitude and the multi-peaked nature of AT 2023txn outburst would nicely fit with a 'Z-And' event, however the appearance of AT 2023txn in quiescence is far from that of classical symbiotic stars in stable burning conditions, which are much brighter than the bare red giant at blue wavelengths and sport a rich esamble of emission lines of both huge intensity and high ionization degree.

Any explanation of the outburst of AT 2023txn needs to account for the simultaneous onset of the deep minima described in sect. 3.4 above, which were absent during the preceding quiescence.

One possibility is that the disk flushes toward the WD its inner portion, which causes the brightness peak. If the inner portion is emptied before any replenishment moves in from outer radii, the brightness of the disk at optical wavelengths will drop to negligible values and the optical photometry and spectroscopy will be dominated by the emission of the bare M6III giant, resulting in the deep minima described in sect. 3.4. If the replenishment on the inner regions is fed by the outer disk in discrete quantities rather than in a smooth and continous way, this could give rise to multiple maxima followed by deep minima as observed in AT 2023txn. In this context, it is worth noticing that also the recent SAP phase of T CrB was modulated in two separated episodes and associated to two distinct brightness maxima (Munari et al. 2025, A&A submitted).

Alternatively, the enhanced mass-flow through the disk of AT 2023txn may have been localized to a range of azimuths, or has given origin to structures extending well above the main plane of the disk, or even may have warped the outer part of the disk. In all these cases, the rotation of the disk may lead the localized structures to cross the line-of-sight to the inner and brighter regions of the disk, producing both the multi-maxima modulation and even total eclipses similar to the observed deep minima.

With the data at hand, useful primarely for the discovery of this interesting new symbiotic star, it seems worthless to venture further with the interpretation of the outburst and deep minima of AT 2023txn. Surely, a protracted monitoring tailored to derive some fundamental parameters like the orbit of the M6III giant and the system inclination in addition to observe the further developments of the outburst, will be crucial to advance our understanding of this object. In addition to encourage future observations in general, we will aim in particoular to acquire regular high-resolution Echelle spectra able to track both the motion of the red giant as well that of the regions from which the emission lines originates.

Acknowledgements. This work has been in part supported by INAF 2023 MiniGrant Program (contract C93C23008470001 to UM). Based in part on observations obtained with the Samuel Oschin Telescope 48-inch and the 60-inch Telescope at the Palomar Observatory as part of the Zwicky Transient Facility project. ZTF is supported by the National Science Foundation under Grant No. AST-2034437 and a collaboration including Caltech, IPAC, the Weizmann Institute for Science, the Oskar Klein Center at Stockholm University, the University of Maryland, Deutsches Elektronen-Synchrotron and Humboldt University, the TANGO Consortium of Taiwan, the University of Wisconsin at Milwaukee, Trinity College Dublin, Lawrence Livermore National Laboratories, and IN2P3, France. Operations are conducted by COO, IPAC, and UW. NM acknowledges financial support through ASI-INAF 2017-14-H.0 agreement (PI: T. Belloni). Part of this work is based on online services provided by the Space Science Data Center - ASI. We also thank Brad Cenko and the Swift Team for the quick approval, scheduling and acquisition of the observation presented in this paper.

References

Bailer-Jones, C. A. L. 2015, PASP, 127, 994
Barentsen, G., Farnhill, H. J., Drew, J. E., et al. 2014, MNRAS, 444, 3230
Bessell, M. S. 1990, PASP, 102, 1181
Blackburn, J. K. 1995, in Astronomical Society of the Pacific Conference Series, Vol. 77, Astronomical Data Analysis Software and Systems IV, ed. R. A. Shaw, H. E. Payne, & J. J. E. Hayes, 367
Breeveld, A. A., Landsman, W., Holland, S. T., et al. 2011, in American Institute of Physics Conference Series, Vol. 1358, Gamma Ray Bursts 2010, ed. J. E. McEnery, J. L. Racusin, & N. Gehrels (AIP), 373–376
Burrows, D. N., Hill, J. E., Nousek, J. A., et al. 2005, Space Sci. Rev., 120, 165
Chen, X., Wang, S., Deng, L., et al. 2020, ApJS, 249, 18
Corradi, R. L. M., Rodríguez-Flores, E. R., Mampaso, A., et al. 2008, A&A, 480, 409
Corradi, R. L. M., Valentini, M., Munari, U., et al. 2010, A&A, 509, A41
Drew, J. E., Greimel, R., Irwin, M. J., et al. 2005, MNRAS, 362, 753
Fitzpatrick, E. L. 1999, PASP, 111, 63
Fujii, M., Kojima, T., Taguchi, K., Kato, T., & Nogami, D. 2023, Transient Name Server Classification Report, 2023-2559, 1
Fujimoto, M. Y. 1982a, ApJ, 257, 767
Fujimoto, M. Y. 1982b, ApJ, 257, 752
Gaia Collaboration. 2016, A&A, 595, A1
Gaia Collaboration. 2023, A&A, 674, A1
Gehrels, N., Chincarini, G., Giommi, P., et al. 2004, ApJ, 611, 1005
Green, G. M., Schlafly, E., Zucker, C., Speagle, J. S., & Finkbeiner, D. 2019, ApJ, 887, 93
Grindlay, J., Tang, S., Los, E., & Servillat, M. 2012, in IAU Symposium, Vol. 285, New Horizons in Time Domain Astronomy, ed. E. Griffin, R. Hanisch, & R. Seaman, 29–34
Henden, A. & Munari, U. 2014, Contributions of the Astronomical Observatory Skalnate Pleso, 43, 518
Hill, J. E., Burrows, D. N., Nousek, J. A., et al. 2004, in Society of Photo-Optical Instrumentation Engineers (SPIE) Conference Series, Vol. 5165, X-Ray and Gamma-Ray Instrumentation for Astronomy XIII, ed. K. A. Flanagan & O. H. W. Siegmund, 217–231
Hodgkin, S. T., Breedt, E., Delgado, A., et al. 2023, Transient Name Server Discovery Report, 2023-2471, 1
Hoffleit, D. 1991, Catalogue of Bright Stars (published by Yale University Observatory)
Iben, I., J. 1982, ApJ, 259, 244
Kenyon, S. J. & Truran, J. W. 1983, ApJ, 273, 280
Koornneef, J. 1983, A&A, 128, 84
Kos, J. & Zwitter, T. 2013, ApJ, 774, 72
Landolt, A. U. 1992, AJ, 104, 340
Landolt, A. U. 2009, AJ, 137, 4186
Lebzelter, T., Mowlavi, N., Lecoeur-Taibi, I., et al. 2023, A&A, 674, A15
Lee, T. A. 1970, ApJ, 162, 217
Luri, X., Brown, A. G. A., Sarro, L. M., et al. 2018, A&A, 616, A9
Mainzer, A., Bauer, J., Cutri, R. M., et al. 2014, ApJ, 792, 30
Mainzer, A., Bauer, J., Grav, T., et al. 2011, ApJ, 731, 53
Masci, F. J., Laher, R. R., Rusholme, B., et al. 2019, PASP, 131, 018003

Morgan, W. W. & Keenan, P. C. 1973, ARA&A, 11, 29
Morgan, W. W., Keenan, P. C., & Kellman, E. 1943, An atlas of stellar spectra, with an outline of spectral classification (University of Chicago Press)
Mukai, K., Luna, G. J. M., Cusumano, G., et al. 2016, MNRAS, 461, L1
Munari, U. 1993, A&A, 273, 425
Munari, U. 2014, in Astronomical Society of the Pacific Conference Series, Vol. 490, Stellar Novae: Past and Future Decades, ed. P. A. Woudt & V. A. R. M. Ribeiro, 183
Munari, U. 2019, in The Impact of Binary Stars on Stellar Evolution, ed. G. Beccari & H. Boffin, arXiv:1909.01389
Munari, U. 2025, Contributions of the Astronomical Observatory Skalnate Pleso, 55, 47
Munari, U., Henden, A., Frigo, A., et al. 2014, AJ, 148, 81
Munari, U. & Zwitter, T. 1997, A&A, 318, 269
Poole, T. S., Breeveld, A. A., Page, M. J., et al. 2008, MNRAS, 383, 627
Predehl, P. & Schmitt, J. H. M. M. 1995, A&A, 293, 889
Rodríguez-Flores, E. R., Corradi, R. L. M., Mampaso, A., et al. 2014, A&A, 567, A49
Roming, P. W. A., Kennedy, T. E., Mason, K. O., et al. 2005, Space Sci. Rev., 120, 95
Sale, S. E., Drew, J. E., Barentsen, G., et al. 2014, MNRAS, 443, 2907
Van Winckel, H., Duerbeck, H. W., & Schwarz, H. E. 1993, A&AS, 102, 401
Wu, C. C., Boggess, A., Bohlin, R. C., et al. 1982, in ESA Special Publication, Vol. 182, Ultraviolet Stellar Classification, ed. A. Heck & B. Battrick, 25–54
Yamashita, Y. & Nariai, K. 1977, An Atlas of representative stellar spectra (Univ. of Tokyo Press)
Zacharias, N., Monet, D. G., Levine, S. E., et al. 2004, in American Astronomical Society Meeting Abstracts, Vol. 205, American Astronomical Society Meeting Abstracts, 48.15

Appendix A: Historical photographic photometry of AT 2023txn

In order to reconstruct the long-term photometric behaviour of AT 2023txn, we have searched the DASCH digitization of Harvard historical photographic plates (Grindlay et al. 2012), which lists data for 2017 plates imaging the field of AT 2023txn over an interval of 88 years, from 1899.776 to 1989.811. A counterpart is detected in only 13 plates, which are given below. To help guessing the confidence on such detections, we also list the closest-in-time plates bracketing each detection.

The supposed detections may either be suspiciously close to plate limit (eg. in 1917.852, 1930.477, and 1938.564), or not confirmed on a similarly deep plate for the following night (1976.585), and they are generally just a single-plate event (which doesn not guarantee against being fooled by plates defects), always of a brightness (much) larger that the peak value characterizing the recent outburst described in this paper.

Overall, the most convincing historical detection seems that of 1952, with AT 2023txn being seen on three plates spanning from August to October, at a mean brightness more in line with that reached at maximum of the recent outburst.

Table A.1: Detection of AT 2023txn on DASCH digitization of Harvard historical photgraphic plates.

HJD	date	mag	err	lim.mag.
2417513.552926	1906.827542	nd		10.69
2417521.559040	1906.849477	12.40	0.28	14.68
2417523.488225	1906.854762	nd		10.42
2421538.474353	1917.846505	nd		10.18
2421540.513781	1917.852093	12.35	0.46	12.43
2421552.476295	1917.884867	nd		12.84
2423647.705041	1923.622480	nd		11.30
2423648.635267	1923.625028	12.08	0.69	12.50
2423649.699234	1923.627943	nd		12.10
2426128.797801	1930.414515	nd		10.76
2426151.804183	1930.477546	12.40	1.25	12.47
2426163.724743	1930.510205	nd		11.12
2429105.636855	1938.564759	nd		13.03
2429105.667248	1938.564842	13.92	0.31	14.45
2429107.634164	1938.570231	nd		11.81
2432803.548437	1948.688657	nd		13.79
2432822.515574	1948.740480	13.58	0.24	16.25
2433044.815646	1949.348810	nd		14.39
2434248.681709	1952.645305	nd		12.53
2434248.745740	1952.645480	14.41	0.10	14.89
2434250.595142	1952.650533	14.52	0.14	14.62
2434290.512226	1952.759596	14.72	0.15	14.93
2434678.612500	1953.822226	nd		12.25
2442684.536111	1975.742565	nd		11.56
2442713.487089	1975.821882	12.68	0.14	14.67
2442902.798160	1976.339612	nd		14.23
2442982.675168	1976.557856	nd		15.11
2442992.697121	1976.585238	13.68	0.14	14.87
2442993.672824	1976.587904	nd		14.88
2446769.492361	1986.926006	nd		13.94
2446915.780265	1987.326795	12.11	0.42	13.14
2446946.821528	1987.411840	nd		12.70
2447242.893403	1988.222386	nd		13.86
2447270.809831	1988.298661	13.79	0.25	14.27
2447330.761806	1988.462464	nd		13.55

Appendix B: gri photometry of AT 2023txn

Some text needed here.

Table B.1: Our *gri* photometry of AT 2023txn.

Date	HJD	*g*	*r*	*i*	ID
2023-10-17.762	2460235.262	13.649 ±0.007	12.092 ±0.006	11.233 ±0.007	0311
2023-12-30.707	2460309.207	14.545 ±0.006	12.827 ±0.007	11.818 ±0.007	0311
2024-01-11.720	2460321.220	14.614 ±0.006	12.863 ±0.004	11.824 ±0.006	0311
2024-01-15.721	2460325.221	14.613 ±0.007	12.877 ±0.005	11.843 ±0.007	0311
2024-01-19.721	2460329.221	14.569 ±0.007	12.865 ±0.005	11.818 ±0.005	0311
2024-01-26.208	2460335.708	14.567 ±0.009	12.856 ±0.008	11.815 ±0.007	0311
2024-01-27.209	2460336.709	14.609 ±0.006	12.856 ±0.006	11.789 ±0.005	0311
2024-01-30.191	2460339.691	14.665 ±0.005	12.911 ±0.006	11.829 ±0.007	0311
2024-02-15.158	2460355.658	14.712 ±0.005	12.970 ±0.006	11.853 ±0.007	0311
2024-02-15.175	2460355.675	14.704 ±0.004	12.966 ±0.006	11.840 ±0.007	0311
2024-02-18.172	2460358.672	14.638 ±0.006	12.883 ±0.008	11.767 ±0.009	0311
2024-02-21.150	2460361.650	14.747 ±0.006	12.974 ±0.009	11.825 ±0.008	0311
2024-03-05.127	2460374.627	14.783 ±0.007	13.004 ±0.005	11.845 ±0.007	0311
2024-03-07.165	2460376.665	14.754 ±0.005	12.988 ±0.007	11.822 ±0.007	0311
2025-05-27.954	2460823.454	17.633 ±0.016	15.031 ±0.010	12.619 ±0.008	0311
2025-06-11.933	2460838.433	16.921 ±0.038	14.615 ±0.023	12.542 ±0.009	0311
2025-06-18.946	2460845.446	16.999 ±0.011	14.720 ±0.008	12.571 ±0.008	0311
2025-06-26.962	2460853.462	16.847 ±0.012	14.617 ±0.008	12.572 ±0.008	0311

Appendix C: Log of spectroscopic observations

Some text needed here.

Table C.1: Journal of the spectroscopic observations of AT 2023txn. The orbital phase in the last column is computed from Eq. 1.

Date	UT	expt	instr.	tel	phase
2023-10-13	20:23	360	B&C	1.22m	0.381
2023-10-14	20:22	2700	Ech	0.84m	0.382
2023-10-27	18:39	2700	Ech	0.84m	0.397
2023-11-08	19:34	3600	Ech	0.84m	0.411
2023-11-13	17:43	480	B&C	1.22m	0.416
2023-11-19	18:29	7200	Ech	0.84m	0.423
2023-12-05	18:00	2700	Ech	0.84m	0.442
2023-12-18	17:17	480	B&C	1.22m	0.457
2023-12-27	18:04	3600	Ech	0.84m	0.467
2024-01-04	17:32	2700	Ech	0.84m	0.476
2024-01-15	17:06	480	B&C	1.22m	0.489
2024-01-16	17:48	2700	Ech	0.84m	0.490
2024-01-27	05:11	1800	Ech	1.82m	0.502
2024-01-29	05:22	1800	Ech	1.82m	0.505
2024-03-12	04:25	2700	Ech	0.84m	0.554
2024-07-11	22:33	600	B&C	1.22m	0.695
2024-09-21	21:15	900	Ech	1.82m	0.778
2024-10-29	19:24	600	B&C	1.22m	0.822
2024-11-15	17:43	600	B&C	1.22m	0.841
2025-03-03	04:07	1200	B&C	1.22m	0.965
2025-06-25	21:35	3600	MMS	0.84m	0.097
2025-06-27	22:30	8100	Ech	0.84m	0.099